

Knowledge Transfer in Engineering Fleets: Hierarchical Bayesian Modelling for Multi-Task Learning

L.A. Bull^{a,*}, M. Dhada^b, O. Steinert^c, T. Lindgren^d, A.K. Parlikad^b, A.B. Duncan^{a,e}, M. Girolami^{a,f}

^aThe Alan Turing Institute, The British Library, London, NW1 2DB, UK

^bInstitute for Manufacturing, Department of Engineering, University of Cambridge, CB3 0FS, UK

^cStrategic Product Planning and Advanced Analytics, Scania CV, Scania AB (publ), SE-151 87 Södertälje, Sweden

^dDepartment of Computer and Systems Sciences, Stockholm University, P.O. Box 7003, SE-164 07 Kista, Sweden

^eDepartment of Mathematics, Imperial College London, London, SW7 2AZ, UK

^fDepartment of Engineering, University of Cambridge, United Kingdom, UK, CB3 0FA

Abstract

We propose a population-level analysis to address issues of data sparsity when building predictive models of engineering infrastructure. By sharing information between similar assets, hierarchical Bayesian modelling is used to improve the survival analysis of a truck fleet (hazard curves) and power prediction in a wind farm (power curves). In each example, a set of correlated functions are learnt over the asset fleet, in a combined inference, to learn a population model. Parameter estimation is improved when sub-fleets of assets are allowed to share correlated information at different levels in the hierarchy. In turn, groups with incomplete data automatically borrow statistical strength from those that are data-rich. The correlations can be inspected to inform which assets share information for which *effect* (i.e. parameter).

Keywords: Hierarchical Bayesian Modelling; Mixed Effects Model; Multi-Task Learning; Structural Health Monitoring; Prognostics and Health Management; Asset Management; Transfer Learning

1. Introduction

Data sparsity can cause significant issues in practical applications of reliability, performance, and safety assessment. Particularly structural monitoring [1], prognostics [2], or performance and health management [3]. In these domains, comprehensive (or high variance [4]) data are rarely available *a priori*; instead, measurements arrive incrementally, throughout the life-cycle of the monitored system [5]. For example, the data recorded from the system in unusual environments, or following damage, might take years to collect. Labelling to annotate the measurements can also be limited or expensive, requiring input from a domain expert. Such incomplete data motivate *sharing* information between similar assets; specifically, whether systems with comprehensive data (or established models) can support those with incomplete information.

The concept of knowledge transfer, from one machine to another, has led to the development of population-based [6–8] or fleet monitoring [9]. Initial investigations (mostly) consider the quantification of *similarity* between systems [7], and tools for the *transfer* of data and/or models from *source* to

target domains [10–12]. An alternative approach is considered here, whereby a combined inference is made from the collected population of fleet data [13]. Specifically, a set of correlated, hierarchic models is learnt, given the information recorded from the collected fleet. Two case studies are presented: survival analysis of an operational truck fleet and wind-power predictions for an operational wind farm. Population-level models are learnt using hierarchical Bayesian modelling [14, 15], providing robust predictions and variance reduction compared to independent models learnt from separated sub-groups of assets. The *multi-task learning* approach [14, 16] automatically shares information between correlated domains (i.e. sub-fleets) such that assets with sparse information borrow statistical strength from those that are data-rich (via correlated variables).

The layout of this paper is as follows. Section 2 summarises existing work relating to population monitoring of engineering systems. Section 3 states the contributions of this work. Section 4 introduces a general methodology for knowledge transfer via hierarchical Bayesian modelling. Sections 5 and 6 present the truck fleet and wind farm case studies. Section 7 offers concluding remarks.

2. Related Work

2.1. Transfer Learning

When monitoring engineering populations, the majority of literature focusses on *transfer learning*. Transfer learning seeks to improve the predictions on a *target domain* given the information in a (more complete) *source domain*. Many examples consider crack detection via image classification using Convolutional Neural Networks (CNNs). For example, Dorafshan *et al.* [17], Gao and Mosalam [18], Jang *et al.* [19] detect cracks over a number of domains by *fine-tuning* the parameters of a CNN trained on a source domain to aid generalisation in the target.

Domain Adaptation is viewed as another variant of transfer learning in engineering applications (DA) [20–22]. These techniques define some mapping from domain data into a shared latent space, where a predictive model is learnt. For example, Michau and Fink [10] apply a neural network mapping for DA in condition monitoring application to a fleet of power plants. DA has also been investigated by (kernelised) linear projection, discussed in a structural health monitoring context by Gardner *et al.* [23, 24] considering methods for knowledge transfer between simulated source and target structures, as well as a simulated source and experimental target structure [25]. Damage detectors have also been transferred between systems using DA in a group of tailplane structures using ground-test vibration data [11].

2.2. Multi-Task Learning

An alternative view of population-level models considers multi-task learning. While the multi-task approach also assumes the predictors (i.e. *tasks*) are similar over the fleet, the parameters across all domains are learnt at the same time with equal importance. A combined inference allows models to share information between related tasks, improving the accuracy in domains where data are limited [26].

Examples of multi-task learning are less prevalent when modelling engineering infrastructure. Wan and Ni [27] successfully use a Gaussian process (GP) to learn correlations between tasks in a multi-output regression. The GP is built using a carefully specified kernel [28] to capture the task and inter-task relationships. The experiments capture correlations between temperature/acceleration sensing systems

on a single structure (the Canton Tower), rather than multiple assets in a fleet. Similarly, Li *et al.* [29] apply correlated GPs to address the missing data problem over multiple sensors of a hydro-electric dam. The results demonstrate successful knowledge transfer between measurement channels. Considering aerospace engines, Seshadri *et al.* [30] apply GPs for knowledge transfer between multiple axial measurement planes when interpolating temperature fields within an aircraft engine. Sharing information between planes significantly improves the spatial representation of the response.

Hierarchical Bayesian modelling offers another multi-task framework. A model is built with a ‘hierarchy’ of parameters, whereby domain-specific tasks are correlated via *shared* latent variables (explained in Section 4). The approach was introduced to structural monitoring by Huang *et al.* [31] and Huang and Beck [32] who utilise hierarchical models to learn multiple, correlated regression models for modal analysis. A shared sparseness profile is inferred over all tasks and related measurements channels, improving damage detection and data recovery by considering the similarity between damage scenarios or adjacent sensors on the same structure. Some recent, related applications include Di Francesco *et al.* [33], who use hierarchical models to build corrosion models given evidence from multiple locations, and Papadimas and Dodwell [34], where the results from a series of materials experiments (i.e. coupon samples) are combined to inform the estimation of material properties.

3. Contribution

The contributions of this work are twofold: (i) multi-task learning with hierarchical Bayesian modelling allows information to be shared between distinct (but related) systems using operational fleet data (wind turbines and trucks) rather than multiple sensors on a single structure; (ii) various *mixed effects* are considered in the hierarchy, such that certain characteristics (parameters) can be learnt at the individual, group, or population level. The hierarchical models are easily formulated around interpretable parameters and the resultant structure allows insightful analyses of the predicted variables, indicating which groups of systems share information for which effect.

4. Hierarchical Bayesian Modelling for Multi-Task Learning with Mixed Effects

We consider fleet data, recorded from a population of engineering systems, which can be separated into K groups or *sub-fleets*. The population data can be denoted,

$$\{\mathbf{x}_k, \mathbf{y}_k\}_{k=1}^K = \left\{ \{x_{ik}, y_{ik}\}_{i=1}^{N_k} \right\}_{k=1}^K \quad (1)$$

where \mathbf{y}_k is target response vector for inputs \mathbf{x}_k and $\{x_{ik}, y_{ik}\}$ are the i^{th} pair of observations in group k . There are N_k observations in each group, and thus $\sum_{k=1}^K N_k$ observations in total. The aim is to learn a set of K predictors, one for each group, related to classification or regression tasks. Without loss of generality, we shall focus on the regression setting, where the tasks satisfy,

$$\{y_{ik} = f_k(x_{ik}) + \epsilon_{ik}\}_{k=1}^K$$

i.e. the output is determined by evaluating one of K latent functions with additive noise ϵ_{ik} . The predictive map f_k can be related to classification or regression tasks.

The mapping f_k is assumed to be similar between sub-fleets. In consequence, the models should be improved by learning the parameters in a joint inference over the whole population. In machine learning, this is referred to as *multi-task learning*; in statistics, such data are usually modelled with hierarchical models [15, 16, 35, 36].

4.1. Hierarchical Bayesian Modelling

In practice, while certain sub-fleets might have rich, historic data, others (particularly those recently in operation) will have limited training data. In this setting, learning separate, independent models for each group will lead to unreliable predictions. On the other hand, a single regression of all the data (complete pooling) will result in poor generalisation. Instead, hierarchical models can be used to learn separate (but correlated) models for each group, while encouraging task parameters to be similar [16].

As an example, consider K linear regression models,

$$\left\{ \mathbf{y}_k = \Phi_k \alpha_k + \epsilon_k \right\}_{k=1}^K \quad (2)$$

where $\Phi_k = [\mathbf{1}, \mathbf{x}_k]$ is the $N_k \times 2$ design matrix; α_k is the 2×1 vector of *weights*; and the noise vector is $N_k \times 1$ and normally distributed¹ $\epsilon_k \sim N(0, \sigma_k^2 \mathbf{I})$. The likelihood of the response is then,

$$\begin{aligned} \mathbf{y}_k | \mathbf{x}_k &\sim N(\Phi_k \alpha_k, \sigma_k^2 \mathbf{I}) \\ \therefore y_{ik} | x_{ik} &\sim N(\alpha_1^{(k)} + \alpha_2^{(k)} x_{ik}, \sigma_k^2) \end{aligned} \quad (3)$$

In a Bayesian manner, one can set a shared hierarchy of prior distributions over the weights (slope and intercept) for each group $k \in \{1, \dots, K\}$,

$$\alpha_k \sim N(\mu_\alpha, \sigma_\alpha^2 \mathbf{I}) \quad (4)$$

$$\mu_\alpha \sim N(\mathbf{m}_\alpha, \mathbf{s}_\alpha \mathbf{I}) \quad (5)$$

$$\sigma_\alpha \stackrel{\text{i.i.d.}}{\sim} \text{IG}(a, b) \quad (6)$$

In words, (4) assumes that the weights $\{\alpha_k\}_{k=1}^K$ are normally distributed $N(\cdot)$ with mean μ_α and covariance $\sigma_\alpha^2 \mathbf{I}$. (A diagonal covariance implies that each model is independent *a priori*.) Similarly, (5) states that the prior expectation of the weights α_k is normally distributed with mean \mathbf{m}_α and covariance $\mathbf{s}_\alpha \mathbf{I}$; (6) states that the prior deviation of the slope and intercept $\{\sigma_{\alpha_j}\}_{j=1}^2$ is inverse-Gamma distributed $\text{IG}(\cdot)$ with shape and scale parameters a and b respectively.

Selecting appropriate prior distributions, and their associated hyperparameters $\{\mathbf{m}_\alpha, \mathbf{s}_\alpha, a, b\}$, is essential to the success of hierarchical models. In this work, we justify these decisions by encoding engineering knowledge in each case study as weakly informative priors [15]. The Directed Graphical Model (DGM) in Figure 1 visualises the general hierarchical regression.

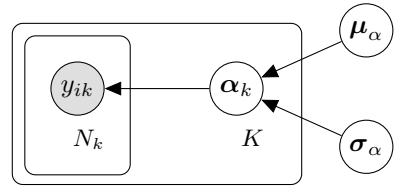


Figure 1: DGM of hierarchical linear regression. The nodes show observed/latent variables as shaded/non-shaded respectively; arrows show conditional dependencies, and plates show multiple instances of subscripted nodes.

The K weight vectors α_k are correlated via the common latent variables $\{\mu_\alpha, \sigma_\alpha^2\}$; i.e. parent nodes in Figure 1. In turn, sparse domains borrow statistical

¹For now, we assume the additive noise σ_k^2 is known. $\mathbf{1}$ is a vector of ones, \mathbf{I} is the identity matrix, and $N(m, s)$ is the normal distribution with mean m and (co)variance s .

strength from those that are data-rich. Crucially, to *share* information between tasks, the parent nodes $\{\mu_\alpha, \sigma_\alpha^2\}$ must be inferred from the population data. This way, the sub-fleet parameters α_k are still (indirectly) influenced by the wider population data. Consider that, if $\{\mu_\alpha, \sigma_\alpha^2\}$ were fixed constants rather than variables inferred from data, each model would be conditionally independent, preventing the *flow* of information between domains [16].

4.2. Mixed-effects modelling

The hierarchical structure allows us to learn *effects* (i.e. interpretable model parameters) at different levels, as well as ‘prior’ information. Specifically, the parameters of the model itself (2) can be learnt at the system, sub-fleet, or population level.

Returning to the regression example (2) we now consider the variance σ_k^2 of the noise ϵ_k to be unknown. While one could learn K domain-specific noise variance terms σ_k^2 , typically, it is assumed that the noise is equivalent across tasks. Sharing the parameter and inferring it from the population can significantly reduce the uncertainty in its prediction. Of course, this assumption should be justified given an understanding of the problem at hand; for example, the same sensing system collects all the population data. In terms of notation, (2) remains the same, however, the domain specific noise vector ϵ_k is now distributed $\epsilon_k \sim N(0, \sigma^2 \mathbf{I})$. Importantly, the removal of subscript- k from the noise variance implies that the size of σ^2 remains the same while the number of the sub-fleets K increases (unlike α_k). Intuitively, σ^2 is now a *tied* parameter [16].

In many applications, it makes sense to infer *effects* at the population level, to further reduce model uncertainty². Throughout this work, we assume these *shared* effects also enter the model linearly,

$$\left\{ \mathbf{y}_k = \underbrace{\Phi_k \alpha_k}_{\text{random}} + \underbrace{\Psi_k \beta}_{\text{fixed}} + \epsilon_k \right\}_{k=1}^K \quad (7)$$

Where Ψ_k is some design matrix of inputs, and β is the corresponding vector of weights. Again, there is no subscript- k for β (like σ^2) as it is tied between subfleets. Following Kreft and De Leeuw [37], we refer to the β coefficients as *fixed effects*, as they are learnt at the population level and shared,

²For example, the intercept would be a shared parameter, with zero-mean, in a related linear regression of Hooke’s law for several materials tests.

while α_k are *random effects*, as they vary between *individuals*. Intuitively, a model with both fixed and random effects can be considered a *mixed* (effects) model [15, 38]. Figure 2 shows the modified DGM of the hierarchical regression. The key differences are nodes outside of the K plate – these are the tied parameters, learnt at the population level.

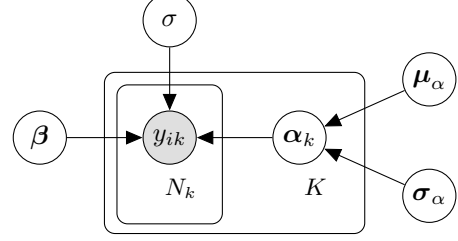


Figure 2: DGM of hierarchical linear regression with mixed effects.

As Gelman *et al.* [15] point out, the terms *random* and *fixed* originate from a frequentist perspective and are somewhat confusing in a Bayesian context where all parameters are random, or (equivalently) fixed with unknown values. We would also like to highlight that interpreting parameter estimates in mixed-effects models can be challenging. If the effects are not (linearly) independent, the fixed and random coefficients can influence each other, making it difficult to reliably recover their relationships. In turn, the modelling assumptions must be carefully considered when emphasising interpretability.

4.3. Inference

In view of graphical models, the observed variables are referred to as *evidence* nodes. For example, the hierarchical regression in Figure 1 would have the following set of evidence nodes,

$$\mathcal{E} = \{[\mathbf{y}_k]\} \quad (8)$$

where $[\mathbf{y}_k]$ is shorthand to denote complete set $\{\mathbf{y}_1, \mathbf{y}_2, \dots, \mathbf{y}_K\}$. On the other hand, the latent variables are *hidden* nodes,

$$\mathcal{H} = \{[\alpha_k], \mu_\alpha, \sigma_\alpha\} \quad (9)$$

Bayesian inference relies on finding the posterior distribution of \mathcal{H} given \mathcal{E} , i.e. the distribution of the unknown parameters given the data,

$$\begin{aligned} p(\mathcal{H}|\mathcal{E}) &= \frac{p(\mathcal{H}, \mathcal{E})}{p(\mathcal{E})} \\ &= \frac{p([\mathbf{y}_k, \alpha_k], \mu_\alpha, \sigma_\alpha)}{p([\mathbf{y}_k])} \\ &= \frac{p([\mathbf{y}_k]|\alpha_k)p([\alpha_k]|\mu_\alpha, \sigma_\alpha)p(\mu_\alpha)p(\sigma_\alpha)}{\int \int \int p([\mathbf{y}_k, \alpha_k], \mu_\alpha, \sigma_\alpha) d\alpha_k d\mu_\alpha d\sigma_\alpha} \end{aligned} \quad (10)$$

DGM representations are useful since inference can be aided by graph-theoretic results. For example, when conditioned on its parents, each node becomes independent of the rest of the graph excluding its descendants. Another example involves Markov blankets – defined as the parents, co-parents, and children of a node. When a node is conditioned on its Markov blanket, it becomes independent from the rest of the graph [14]. The systematic application of graph-theoretic algorithms has led to a number of probabilistic programming languages – here, we implement models in `Stan` [39]. The parameters are inferred using MCMC, via the no U-turn implementation of Hamiltonian Monte Carlo [40]. Throughout, the burn-in period is 1000 iterations, and 2000 iterations are used for inference. Code based on the first case study is publicly available on GitHub³.

4.4. Engineering applications

In each case study, we formulate hierarchical models for knowledge transfer between asset models. The first concerns survival analysis of truck fleets (hazard curves) and the second concerns power prediction for turbines (power curves). In each study, we encode engineering expertise in a number of ways: to (i) inform prior elicitation, (ii) determine which effects are random or fixed, and (ii) formulate interpretable parameters. In turn, population modelling offers insights as to which sub-fleets share information for which (interpretable) effect.

Most importantly, by considering the collected population, we can, in effect, extend the training data. In turn, parameter estimation can be improved while increasing the reliability of predictions. There are, of course, important considerations when building such models – prior elicitation, mixed-effects formulation, negative transfer – these concepts are discussed throughout.

5. Truck-Fleet Survival Analysis

This study concerns the survival analysis of components (alternators and turbochargers) in a fleet of heavy-duty trucks owned by Scania CV. The components are maintained in a run-to-failure strategy, as failure prediction models are unavailable and it is infeasible for drivers to sense incipient failure.

Nonetheless, the associated downtime can incur high costs: relating to late goods delivery, re-loading, and towing vehicles to the workshop.

For such components, survival analysis [2] is critical to estimate the time to failure, and therefore fundamental when designing a maintenance plan. The analysis considers failure occurrences in the population over some specified time period. The period must be sufficiently long, such that reliability functions can be evaluated based on the observed failures or drop-outs [41]. Here, we focus on the hazard function which defines the instantaneous rate of failure. Specifically, hazard $\lambda(t)$ is the probability of a component failing at time t , given that it has survived until time t [41],

$$\lambda(t) = \frac{P(t \leq T < t + dt | T \geq t)}{dt} \quad (11)$$

here T denotes the *time of failure*. Empirically, this is calculated as the fraction of trucks that failed to the number of trucks that survived, in a given time interval. It is important to note, each sample from the reliability function requires at least one failure in the historic fleet data. For this reason, if failures are rare in certain sub-fleets, the data that represent the corresponding function will be sparse. This fact motivates sharing information between hazard curve relationships.

The hazard data for truck fleet alternators are shown in Figure 3. Herein, we work with the log-hazard, since it is easier to visualise and relate to interpretable parameters (introduced in Section 5.1). There are 437 observations in total, split into a 75% training set and 25% test set. The data are normalised, with axis details removed throughout in view of data sensitivity. The sub-fleets were manually labelled in collaboration with the engineers at Scania. Colours correspond to different sub-populations, where the total number of groups (and, therefore, hazard functions) is $K = 8$. Note that certain domains are more sparse than others, with the most extreme case being $k = 8$, which owns a single observation. The population model will look to utilise data-rich domains with more information ($k \in \{1, 2, 3\}$) to support the sparse domains ($k \in \{5, 6, 7, 8\}$). The number of observations of each task are as follows,

N_1	N_2	N_3	N_4	N_5	N_6	N_7	N_8	$\sum_{k=1}^K N_k$
180	108	70	49	15	7	7	1	437

³Rather than the operational data presented here, the code uses simulated data (in view of data sensitivity).

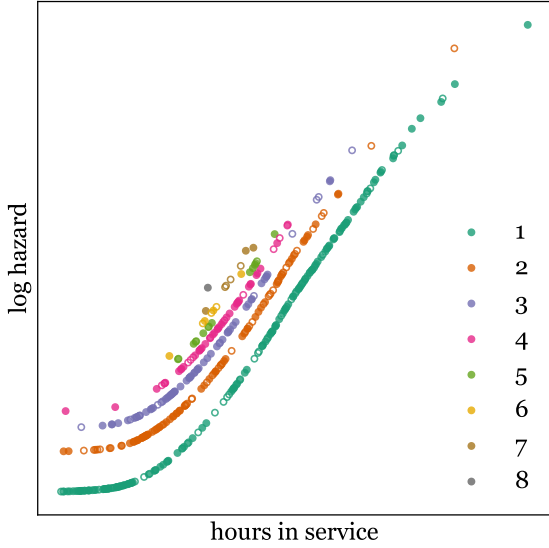


Figure 3: Log hazard function data for alternators in the truck fleet. Training and testing markers are \bullet and \circ respectively. Colours correspond to sub-fleet labels.

5.1. Task regression formulation

When analysing survival data, it is convenient to assume the survival time T is parametrically distributed since the parameters are interpretable and formulate a specific hazard function. A straightforward example is presented when T is exponentially distributed, leading to a constant hazard [42].

Rather than constant, Figure 3 shows the log-hazard is near-linear for a large proportion of the input domain, with a notable nonlinear effect at low t values (early hours in service). We therefore assume the best (parametric) approximation of the marginal $p(T = t)$ is the Gompertz distribution (G) for each sub-fleet [42],

$$\begin{aligned} p(T = t) &= G(t; \gamma, \phi) \\ &= (\gamma e^{\phi t}) \exp \left\{ -\frac{\gamma}{\phi} (e^{\phi t} - 1) \right\} \end{aligned} \quad (12)$$

This is convenient, since (12) is formulated such that log-hazard is linear in time t ,

$$\begin{aligned} \log \lambda_G(t) &= \log \gamma + \phi t \\ &= \alpha_1 + \alpha_2 t \end{aligned} \quad (13)$$

Since hazard data were available in this study, we fit tasks using a hazard representation, relating to (13), rather than the distribution (12). For a better interpretation of the parameters in practice, we would recommend fitting the population model directly to the distribution over the time-at-failure T .

In view of the data in Figure 3, we use weighted sum of H B-spline bases functions $b_h(t)$ to model

the (non-parametric) discrepancy between the linear Gompertz hazard and the empirical data,

$$\begin{aligned} \log \lambda(t) &= \alpha_1 + \alpha_2 t + \sum_{h=1}^H \beta_h b_h(t) \\ &= \log \lambda_G(t) + \sum_{h=1}^H \beta_h b_h(t) \end{aligned} \quad (14)$$

We select cubic B-splines (Appendix A) as they are smooth with compact support, resulting in a sparse design matrix for the β_h terms⁴ [15]. This property is suitable since the nonlinear response acts in specific (compact) regions of the input. In effect, (14) defines a semi-parametric (or a partially-linear) regression [14] with kernel smoothing to approximate the hazard functions for each sub-fleet.

5.2. Mixed-effects formulation

From Figure 3, one observes the underlying linear trend $\{\alpha_1 + \alpha_2 t\}$ is similar (but varied) between sub-fleets while the nonlinear effect $\sum_{h=1}^H \beta_h b_h(t)$ appears consistent over the population. In other words, while the data are poorly described by a (linear) Gompertz hazard function, the (nonparametric) discrepancy remains consistent.

We therefore assume the associated spline weights $\beta = \{\beta_h\}_{h=1}^H$ are fixed effects and learnt at the population level. On the other hand, task-specific linear weights are inferred, $\alpha_k = \{\alpha_1^{(k)}, \alpha_2^{(k)}\}$, which are correlated via common latent variables (random effects).

Our mixed effect model can now be expressed in the general notation from (7),

$$\left\{ \mathbf{y}_k = \underbrace{\Phi_k \alpha_k}_{\text{random}} + \underbrace{\Psi_k \beta}_{\text{fixed}} + \epsilon_k \right\}_{k=1}^K$$

Specifically, for each sub-fleet k : \mathbf{y}_k is the output of the log-hazard (14) with additive noise ϵ_k ; \mathbf{x}_k are the inputs corresponding to time t ; α_k is the varying linear weight vector with design matrix $\Phi_k = [\mathbf{1}, \mathbf{x}_k]$; and β is the tied/fixed weight vector, with a design matrix of splines,

$$\Psi_k = [b_1(\mathbf{x}_k), b_2(\mathbf{x}_k), \dots, b_H(\mathbf{x}_k)] \quad (15)$$

The resultant graphical model corresponds to Figure 2.

⁴An appropriate number of splines H will be determined through cross-validation.

5.3. Weakly informative priors

Primarily considering α_k , it is possible to encode prior knowledge of the expected functions, since the linear component corresponds to a Gompertz survival model (13). It is acknowledged that, in this case, the specific hyperparameter values are less meaningful as the data are normalised; however, their interpretation remains relevant.

Specifically, α_k is distributed according to equations (4) to (6), with hyperparameters,

$$\mathbf{m}_\alpha = [0, 1.5]^\top, \quad \mathbf{s}_\alpha = [2, 0.5]^\top \quad (16)$$

$$a = 1, \quad b = 1 \quad (17)$$

The first element of \mathbf{m}_α corresponds to the intercept and postulates the baseline log-hazard⁵. (This is 0 since the data are centered). The second element of \mathbf{m}_α is the expected slope of the log-hazard. (Set to 1.5 as we expect hazard to increase exponentially under the Gompertz model with a gradient > 1 when normalised). The \mathbf{s}_α values indicate a weakly informative prior under the ranges imposed by z-score normalisation. Similarly, the a, b values encourage correlation between sub-fleet models, such that the prior mode of the standard deviation of the generating distribution of α_k is $b/(a+1) = 1/2$ (this intentionally overestimates the deviation σ_α between sub-fleets, such that the population model weakly constrains α_k).

The shared prior over the variance of the additive noise ϵ_k is set to,

$$\sigma \sim \text{IG}(3, 0.8) \quad (18)$$

Whose mode is at 0.2, indicating that we expect the standard deviation of the noise to be significantly less (around five times) than that of the output, i.e. a high signal-to-noise ratio.

Following a standard approach [15] the basis function model can be centered around the linear component ($\log \lambda_G(t)$) via specification of the β prior. Specifically, we postulate a *shrinkage* prior with a high density at zero, to (effectively) exclude basis functions by encouraging their expected posterior weights to be near-zero – while also having heavy tails to avoid over-shrinkage. A standard hierarchical prior is used [15] which exhibits these desired properties,

$$\beta_h \sim \text{N}(0, \sigma_h^2), \quad \sigma_h^2 \sim \text{IG}(v, v) \quad (19)$$

⁵Or the exponentiated initial rate-of-failure.

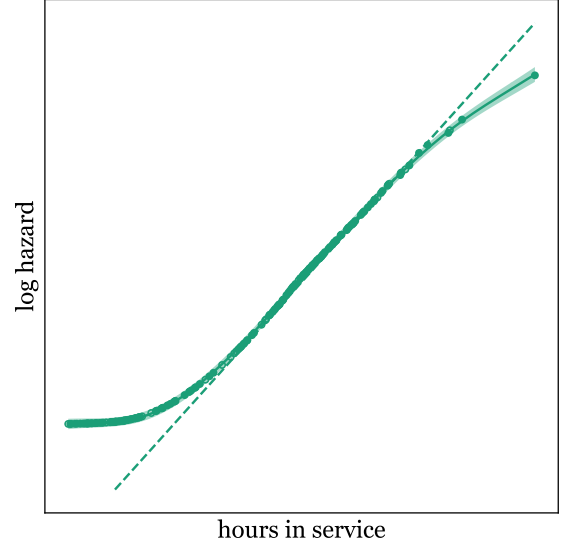


Figure 4: Basis function model for the data-rich domain ($k = 1$). The Gompertz (linear) fit is shown by the dashed line (equation (13)) and the posterior mean is shown by the solid line (equation (14)). The number of splines H is selected by 20-fold cross-validation.

where v is some small nonzero value – in this case $v = 10^{-3}$.

To summarise, without any data, our prior postulates that we expect to see an underlying linear log-hazard, corresponding to a Gompertz survival model (13). The discrepancy between this simple (parametrised) behaviour and the data will be modelled by nonparametric splines, resulting in a semi-parametric regression (14) for each task. Figure 4 visualises the implications of the model and prior, which shows the posterior predictive distribution inferred from the most data-rich domain only ($k = 1$, single-task learning). This experiment is used to validate an appropriate number of splines for the population model, which is found to be $H = 5$ through 20-fold cross-validation, presented in Appendix B. It is intuitive to note, the same independence can, in effect, be achieved for parameters with hierarchical priors (i.e. α_k) by letting the variance of their generating distribution become very large [24] (i.e. $\sigma_\alpha \rightarrow \infty$).

5.4. Results

To motivate sharing information within the fleet, we first learn the regression task for each sub-fleet independently. This corresponds to learning separate (task-specific) parameters, which are independent, preventing the flow of information via correlated variables or tied parameters. The separated models can be visualised by removing the K plate from the

DGM in Figure 2, while including k -subscripts for σ^2 and β . Figure 5 presents these updates.

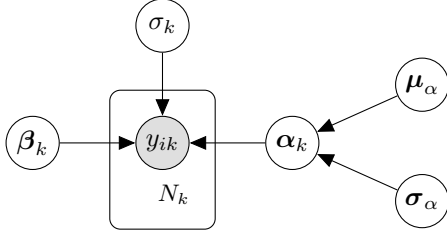


Figure 5: DGM for independent linear models.

Figure 6 shows the resulting domain-wise regression (i.e. single task learning). The posterior-predictive distributions $p(\mathbf{y}_k^* | \mathbf{x}_k^*, \mathbf{x}_k, \mathbf{y}_k)$ make sense under the model/prior formulation, however, independent models fail to consider that valuable information might be shared between the task relationships. In turn, the posterior predictive distribution presents large uncertainty, especially in sparse domains.

We now apply hierarchical modelling to learn the parameters in a combined inference from the population data. The mean and standard deviation of samples drawn from the multi-task learning posterior predictive distribution are shown in Figure 7. Visually, the predictive distributions $p(\mathbf{y}_k^* | \mathbf{x}_k^*, \{\mathbf{x}_k, \mathbf{y}_k\}_{k=1}^K)$ better represent our belief of the underlying task functions by leveraging information between domains. In particular, information from data-rich domains ($k \in \{1, 2, 3, 4\}$) informs the (fixed) nonlinear effect.

The predictive (log) likelihood for out-of-sample test data (25%) is evaluated for a large number of trials (100) via bootstrap sampling. The average population log-likelihood increases significantly, from 355 to 410, highlighting improvements following inference at the fleet level. Table 1 presents the relative changes for each task, where STL is single-task learning and MTL is multi-task learning⁶. There is a relative improvement in all domains (other than $k = 7$) especially those domains with sparse training data. A notable increase is for $k = 2$ since leveraging information enables more reliable extrapolation (to late hours in service) where the test data are likely to be sparse. We believe a likelihood decrease occurs in domain $k = 7$, since the sub-fleet labelling may be unreliable – the hazard data could in fact represent more than one group when observing Fig-

ure 3. Improvements to the labelling procedure are discussed as future work, Section 7.

Table 1: Out-of-sample (average) predictive log likelihood for 25% test data: $\log p(\mathbf{y}_k^* | \mathbf{x}_k^*)$

model	$k = 1$	$k = 2$	$k = 3$	$k = 4$	$k = 5$	$k = 6$	$k = 7$
STL	150.24	94.24	57.66	47.04	8.51	-3.17	0.95
MTL	166.18	98.23	64.78	58.09	25.7	10.17	-13.58

We also consider reductions in the posterior variance of the parameters when multi-task learning. Figures 8 and 9 show the posterior distribution of the slope and intercepts respectively: these parameters correspond to the random (linear) effect of the Gompertz model $\alpha_1 + \alpha_2 t$ (13). Variance reductions are most significant in sparse domains (bottom row) and less significant in the data-rich domains (top row). This follows intuition since the population model allows sparse domains to *borrow* information via the shared parent nodes $\{\mu_\alpha, \sigma_\alpha^2\}$ while the data-rich domains are largely unaffected.

Figure 10 shows the posterior distribution of the fixed weights β . Under the prior specification, these weights adaptively deviate from zero to model the discrepancy from the linear effect in sparse/compact regions of the input (via nonparametric splines). Building on intuition, by tying these parameters, the expected values shift towards the expectation of the data-rich, independent models ($k \in \{1, 2, 3, 4\}$). In other words, in the population-level inference, the fixed effect is learnt from the domains which have data to describe it.

Likewise, Figure 11 shows improvements in the estimate of $\sigma_{(k)}$ when tying the noise effect. The posterior variance is reduced, while the expected values indicate a lower noise variance. This should be expected since by pooling the data to learn $\sigma_{(k)}$ we effectively extend our training set; in turn, the posterior moves further away from our weakly informative prior (18).

5.5. Modelling additional failures and the risk of negative transfer

The assumptions which select the tied parameters are critical – this caveat is widely acknowledged. If any assumptions prove inappropriate or non-general, the multi-task learner can risk negative transfer, whereby predictions are worse than conventional (i.e. single-task) learning – i.e. in this case, independent models. To highlight this concern, we consider empirical hazard data from another component

⁶Domain $k = 8$ is excluded since there is only one observation in the historic fleet data.

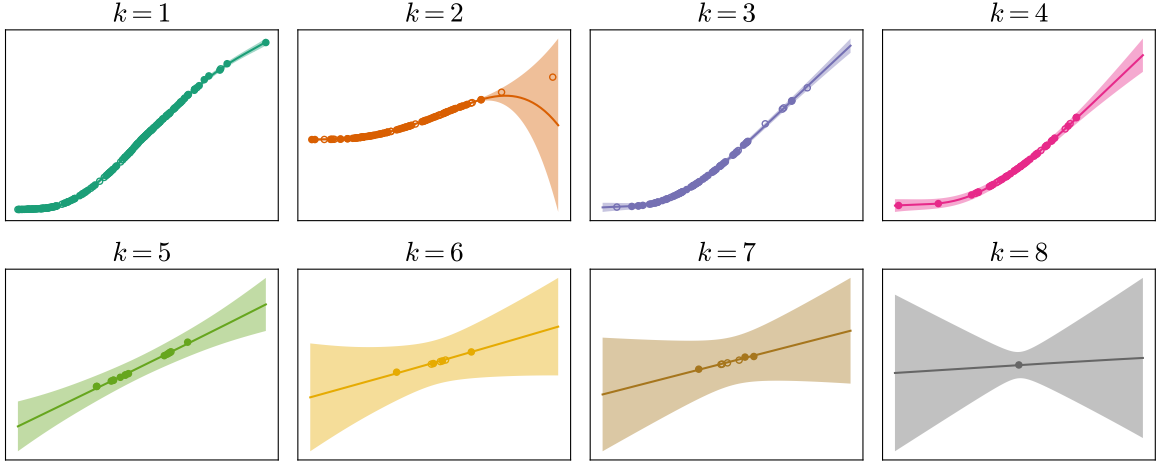


Figure 6: Posterior predictive distribution $p(\mathbf{y}_k^* | \mathbf{x}_k^*, \mathbf{x}_k, \mathbf{y}_k)$: the mean and three-sigma deviation for K independent regression models.

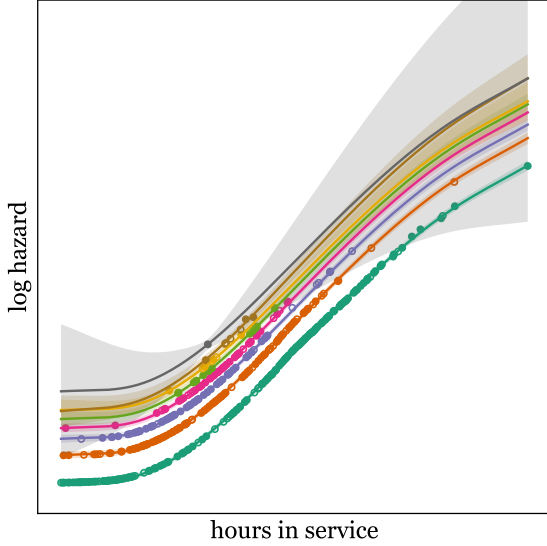


Figure 7: Posterior predictive distribution $p(\mathbf{y}_k^* | \mathbf{x}_k^*, \{\mathbf{x}_k, \mathbf{y}_k\}_{k=1}^K)$: the mean and three-sigma deviation for multitask learning with mixed effects.

in the same fleet of vehicles, turbochargers. The survival data are presented Figure 12, which are calculated following the same procedure as the alternators.

Critically, manually labelling the alternator data is problematic, since it becomes infeasible to categorise observations as the generating functions become more compact, or towards the end of the operational life. The associated *unlabelled* data are highlighted with small \circ markers in Figure 12. There are various options when considering these data. One could treat the observations as a single (pooled) sub-fleet or task, with a large expected variance; alternatively, the labels themselves could be treated as an additional latent variable, such that categorisation

into task groups is unsupervised. Here, we opt to remove the unlabelled data during preprocessing, since modelling them is out of the scope of this work; alternative solutions are proposed in the concluding remarks Section 7. The resulting turbocharger dataset has 287 (normalised) observations over six tasks, such that $k \in \{1, 2, \dots, 6\}$, and the number of observations in each domain is as follows,

N_1	N_2	N_3	N_4	N_5	N_6	$\sum_{k=1}^K N_k$
112	60	32	28	25	30	287

As before, the data are split into 75% training and 25% test sets.

From Figure 12, one observes that the turbocharger hazard data are similar to Figure 3 (alternators). Since the components operate within the same fleet of vehicles, we assume that information can be shared between the associated predictors by extending the task-set in the hierarchic model. A naïve approach assumes the same formulation of mixed effects, this simply extends the total number of tasks such that $K = 14$ (i.e. $8 + 6$) and infers the parameters from both alternator and turbocharger hazard data. Appendix D presents the posterior predictive distribution of such a model. While the model interpolates well, the extrapolation behaviour⁷ is problematic for later hours in service. This is because the model assumes that the discrepancy (from the Gompertz model) is equivalent for both components, as the nonparametric weights β remain tied over all tasks. The unlabelled data are evidence

⁷At the population level, this is not extrapolation, since we learn the response at late hours in service from the alternator domain.

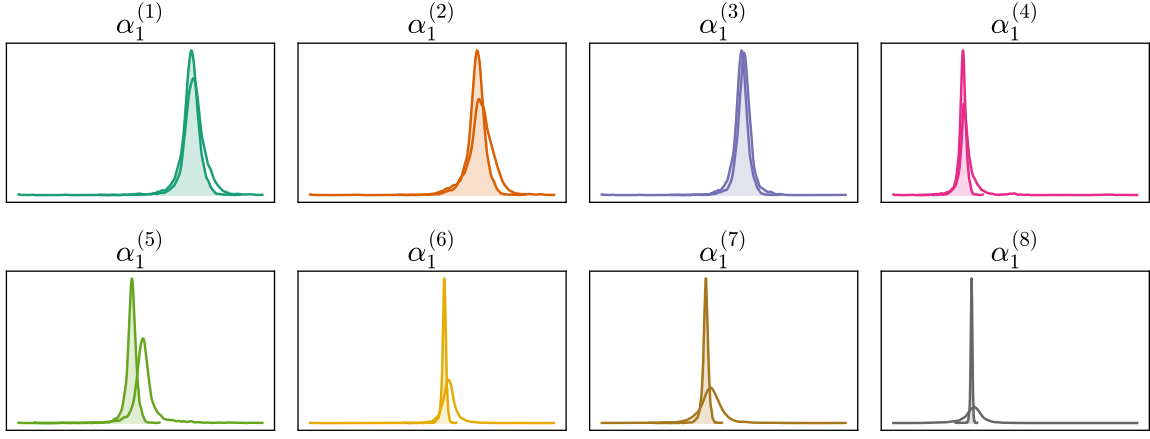


Figure 8: Variance reduction in the posterior distribution of the intercept parameters $\alpha_1^{(k)}$. Independent models (hollow) compared to population-level modelling (shaded).

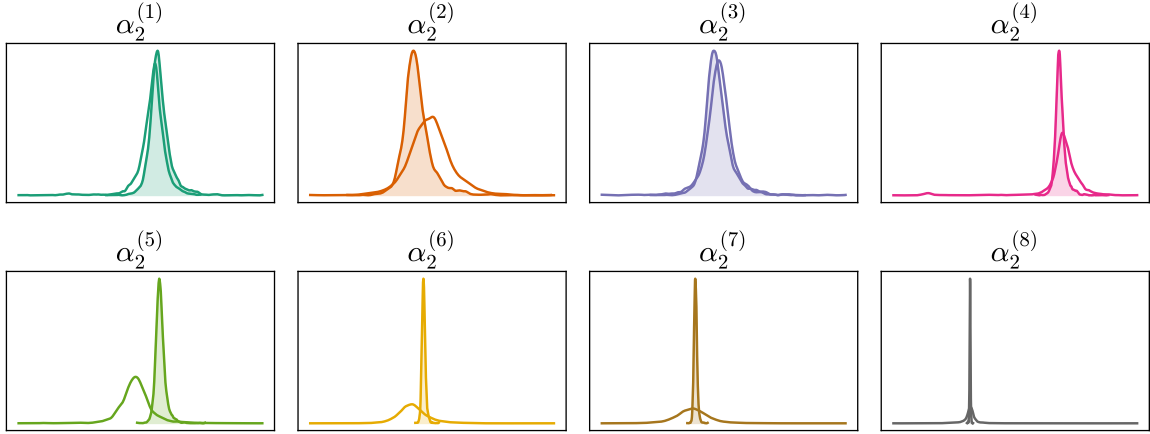


Figure 9: Variance reduction in the posterior distribution of the slope parameters $\alpha_2^{(k)}$. Independent models (hollow) compared to population-level modelling (shaded).

that this assumption is inappropriate, as the model would generalise poorly to these data, plotted in Appendix D. The resultant model would have a high risk of negative transfer.

Instead, we reformulate the mixed effect model, whereby a separate, nonparametric discrepancy $\{\beta_l\}_{l=1}^L$ is learnt for the alternator ($l = 1$) and turbocharger ($l = 2$) tasks – introducing two higher-level subgroups, such that $L = 2$. As before, the parameters of the linear component remain correlated via the shared parent nodes, allowing knowledge transfer between all 14 tasks (both alternators and turbochargers). In turn, our model and prior now postulate a similar but varying underlying linear trend for all tasks (the Gompertz model); however, the discrepancy from this behaviour is component-specific (a separate β_l for each component). The modifications can be visualised by updating the DGM from Figure 2 to include higher-level sub-

groups $l \in \{1, 2\}$, presented in Figure 13, where $l = 1$ alternators or $l = 2$ turbochargers. A key difference is the new L -plate and the associated subscripts: K_l is the number of sub-fleets for each component, such that $K_1 = 8$ (alternators) or $K_2 = 6$ (turbochargers); while β_l indicates a separate (independent) weight vector for each component. The collected tasks become,

$$\left\{ \left\{ \mathbf{y}_{kl} = \underbrace{\Phi_{kl}\alpha_k}_{\text{random}} + \underbrace{\Psi_{kl}\beta_l}_{\text{fixed}} + \epsilon_{kl} \right\}_{k=1}^{K_l} \right\}_{l=1}^L \quad (20)$$

Figure 14 plots the mean and standard deviation of samples drawn from the posterior distribution of the extended population model (compared to independent turbocharger models). By specifying component-specific weights β_l , the representation of uncertainty improves when extrapolating in the turbocharger domain. We also observe reductions in

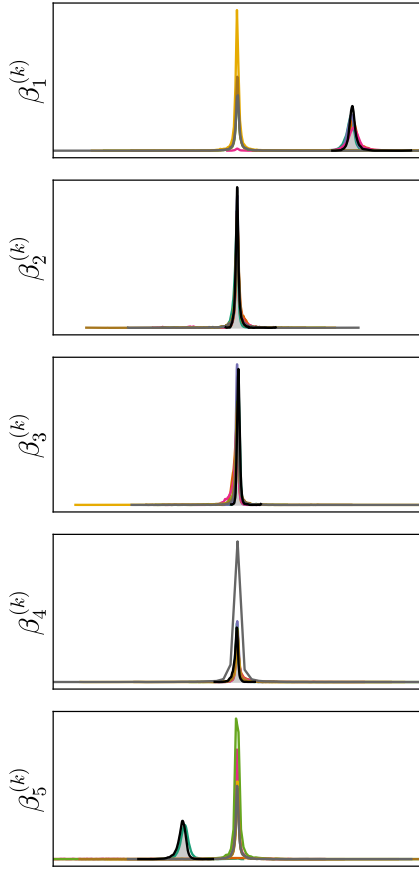


Figure 10: Posterior distribution of the weight parameters $\beta_{(k)} = \{\beta_h^{(k)}\}_{h=1}^H$. Comparison between the tied population-level parameters (grey shaded) and independent models (hollow) for each domain $k \in \{1, \dots, 8\}$.

the posterior predictive distribution $p(\mathbf{y}_{kl}^* | \mathbf{x}_{kl}^*)$ (ignoring all conditionals) for alternator tasks ($l = 1$) since the population data have been extended for the linear component. Likewise, variance reductions are observed in the posterior distributions of the intercept and slope, visualised in Appendix E.

Fleet-level inference improves the (bootstrapped) predictive log-likelihood from 570 to 646, highlighting improvements in predictive capability for the combined fleet over both components. The task-wise predictive likelihood is presented in Table 2 for the alternator ($l = 1$) and turbocharger ($l = 2$) domains. Note, however, that the likelihood fails to increase for certain alternator tasks ($k = 1$ or 5) reiterating the risk of negative transfer in the extended model. Ideally, the dataset should be much larger to determine if negative transfer has occurred and whether the current assumptions are appropriate.

Figure 15 is insightful since it informs which correlations in the hierarchy *transfer* or *share* information between the sub-fleet (k) or component (l) groups. The heat-map corresponds to the Pearson

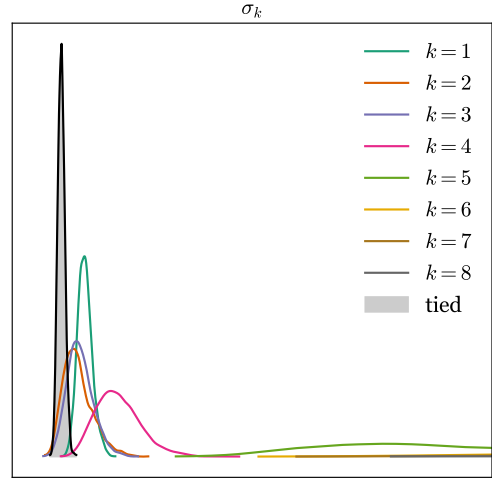


Figure 11: Posterior distribution of the noise parameter $\sigma_{(k)}$. Comparison between the tied population-level parameters (grey shaded) and independent models (hollow) for each domain $k \in \{1, \dots, 8\}$.

Table 2: Out-of-sample (average) predictive log likelihood for 25% test data, $\log p(\mathbf{y}_{kl}^* | \mathbf{x}_{kl}^*)$. Here l corresponds to the component label (alternator $l = 1$ or turbocharger $l = 2$) while k is the sub-fleet label for each component.

	model	$k = 1$	$k = 2$	$k = 3$	$k = 4$	$k = 5$	$k = 6$	$k = 7$
$l = 1$	STL	150.24	94.24	57.66	47.04	8.51	-3.17	0.95
$l = 1$	MTL	164.54	96.98	62.79	57.51	24.7	11.12	-9.13
$l = 2$	STL	90.37	48.35	21.63	17.13	13.73	23.74	-
$l = 2$	MTL	81.34	53.14	35.97	23.94	11.2	32.17	-

correlation coefficient of the posterior distribution between variables that share parent nodes in the graphical model (i.e. α_{kl}) – these correlations enable multi-task learning. Intuitively, Figure 15a shows increased correlation between the intercepts of the same component, with two clear blocks of 8×8 (alternators) and 6×6 (turbochargers). The intercept correlation structure is interpretable since components of the same type are likely to have a similar baseline hazard.

The slope correlation structure in Figure 15b is more descriptive. In the top left block, the alternators are less correlated as the domains become more sparse (from $1 \rightarrow 8$); this makes sense since the level of correlation is reduced where there are fewer data to support task similarity. The effect is most obvious for $k = 8$ (alternators) which only has a single training point. In both Figures 15a and 15b, the structured covariance of α_{kl} highlights how inter-task correlation contributes to variance reduction in the fleet-model.

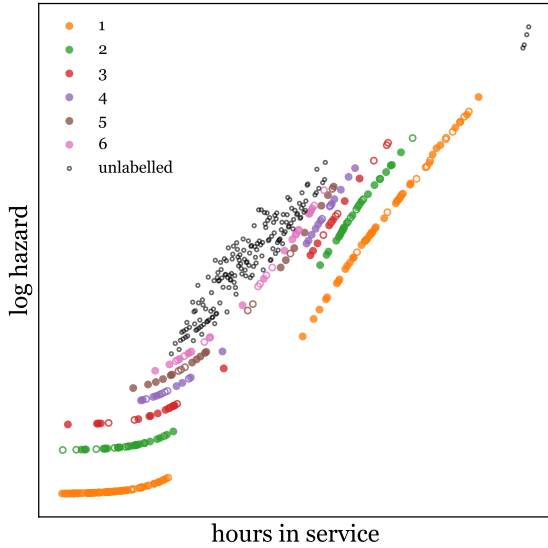


Figure 12: Log hazard data for turbochargers in the truck fleet. Training and testing markers are \bullet and \circ respectively. Colours correspond to sub-fleet labels.

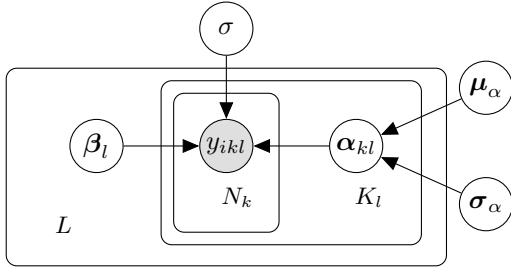


Figure 13: DGM of hierarchical linear regression with mixed effects. Introducing a higher-level group, such that the total number of tasks is $L \times K_l$.

6. Wind Farm Power Prediction

To demonstrate the applicability of hierarchical models, we now consider power prediction in a wind farm case study. Here the regression tasks f_k are *power curves*, which map from wind speed to power output for a specific turbine [43]. The associated function can be used as an indicator of performance and is useful in monitoring procedures [44]. Data-based methods approximate this relationship from operational measurements, typically recorded using Supervisor Control and Sensory Data Acquisition (SCADA) systems [45]. Various techniques have been proposed to model data that correspond to *normal* operation [46–48]. In practice, however, only a subset of measurements represent this relationship. In particular, power *curtailments* will appear as additional functional components; these usually correspond to the output power being controlled (or otherwise limited) by the operator. Reasons for this action include: adhering to the requirements of the electrical grid [49, 50], the mitigation of load-

ing/wake effects [51], and restrictions enforced by planning regulations.

Figure 16 shows power curve data, including curtailments, provided by Visualwind and recorded from three operational turbines. The turbines are the same make and model but in different locations. As before, the data are normalised with axis values removed throughout in view of data sensitivity. The work in [52] demonstrates a suitable method to represent similar normal and curtailed functions in a combined model; however, each function f_k is assumed independent – in turn, there is no knowledge transfer between task parameters. Here, we enable knowledge transfer by correlating the regression models in a hierarchical formulation.

There are 12,231 observations in total. The data were labelled in weekly subsets, according to turbine $k \in \{1, 2, 3\}$ and operational condition (normal or curtailed) $l \in \{1, 2\}$. Each point corresponds to a 10-minute average of power y_{ikl} and wind speed x_{ikl} . The first turbine has 2 weeks of data, the second has 7.5 weeks, and the third has 11.5 weeks. Missing values and very sparse outliers were removed from the dataset (using the local outlier factor algorithm [53]). Since the first turbine presents a normal power curve only ($l = 1$) there is a total of five tasks, $\sum_{l=1}^L K_l = K_1 + K_2 = 3 + 2 = 5$. As before, specific tasks have less data than others, with the number of observations per group is as follows,

	N_{1l}	N_{2l}	N_{3l}	$\sum_{k=1}^{K_l}$
normal ($l = 1$)	1073	3519	5850	10442
curtailed ($l = 2$)	-	636	1153	1789

The proportions of training data are listed below. The observations remain ordered to test generalisation to measurements from later operational life.

$k = 1$	$k = 2$	$k = 3$
90%	66%	66%

The splits are intentionally inconsistent, to allow a combined inference to leverage information from the data-rich tasks (with historic data) to support sparse tasks (systems recently in operation). In particular, referring to Figure 16: the normal data from the first turbine ($k = 1, l = 1$: dark blue) should support the sparse normal tasks ($k \in \{2, 3\}$: dark orange and green); while the data-rich curtailment from the third turbine (light green) should support the curtailed relationship of the second turbine (light orange).

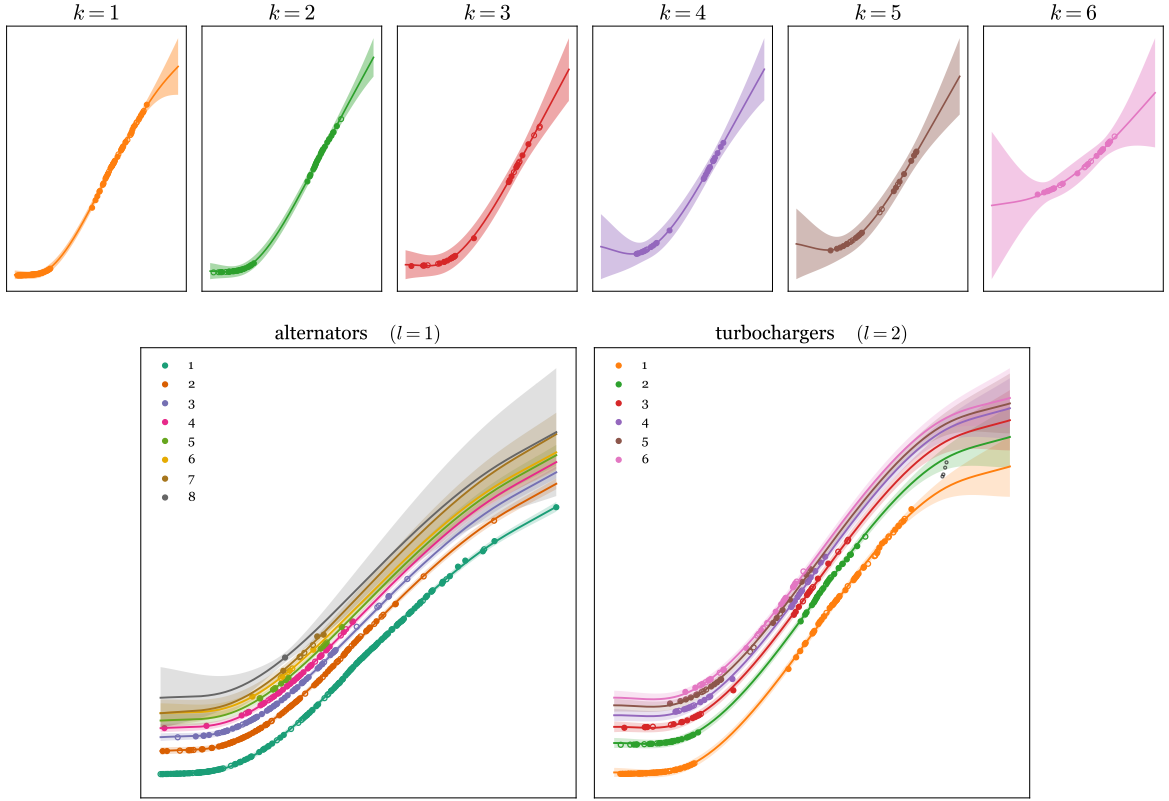


Figure 14: Posterior predictive distribution, the mean and three-sigma deviation for: (top) K independent regression models of turbocharger hazard $p(\mathbf{y}_{kl}^* | \mathbf{x}_{kl}^*, \mathbf{x}_{kl}, \mathbf{y}_{kl})$. (bottom) multitask learning with mixed effects for all turbocharger and alternator tasks $p(\mathbf{y}_{kl}^* | \mathbf{x}_{kl}^*, \{\{\mathbf{x}_{kl}, \mathbf{y}_{kl}\}_{k=1}^{K_l}\}_{l=1}^L)$.

6.1. Task regression formulation

A standard power curve model assumes segmented linear regression [48], here we adopt a similar formulation,

$$P(x_i) = \begin{cases} 0 & x_i < p \\ m_1(x_i - p) & p < x_i < q \\ m_2(x_i - q) + m_1(q - p) & q < x_i < r \\ P_m & x_i > r \end{cases}$$

$$m_2 \triangleq \frac{P_m - m_1(q - p)}{(r - q)} \quad (21)$$

Although simple, (21) presents interpretable parameters – visualised in Appendix C. p is the cut-in speed and r is the rated speed; the change-point q corresponds to the initiation of the limit to maximum power P_m (where $p < q < r$). The gradients m_1 and m_2 approximate the near-linear response between p - q and q - r respectively. The second change point and gradient $\{q, m_2\}$ enable *soft* curtailments, rather than a hard-limit at maximum power P_m .

6.2. Mixed-effects and prior formulation

From knowledge of turbine operation, the expected power before cut-in should be zero for all turbines

(i.e. a fixed effect). The cut-in speed p is also tied as a fixed effect and learnt at the population level since all turbines have the same design. Similarly, the max power P_m is tied between operational labels $l \in \{1, 2\}$ such that one parameter is learnt for the normal tasks ($l = 1$) and one for the curtailed tasks ($l = 2$). Conversely, the change-points $\{q, r\}$ and gradients $\{m_1, m_2\}$ are assumed similar but varying between all tasks, i.e. correlated via shared parent nodes. In turn, one would expect the curtailed relationships ($l = 2$) to be more correlated (and share more information) than the normal relationships ($l = 1$), and vice versa.

We summarise the collected tasks as segmented mixed effects

$$\left\{ \left\{ y_i^{(kl)} = \begin{cases} 0 & x_i < p \\ m_1^{(kl)}(x_i - p) & p < x_i < q^{(kl)} \\ m_2^{(kl)}(x_i - q^{(kl)}) + m_1^{(kl)}(q^{(kl)} - p) & q^{(kl)} < x_i < r^{(kl)} \\ P_m^{(l)} & q^{(kl)} < x_i < r^{(kl)} \end{cases} \right. \right. \\ \left. \left. \dots + \epsilon_i^{(kl)} \right\}_{k=1}^{K_l} \right\}_{l=1}^L$$

$$m_2^{(kl)} \triangleq \frac{P_m^{(l)} - m_1^{(kl)}(q^{(kl)} - p)}{(r^{(kl)} - q^{(kl)})} \quad (22)$$

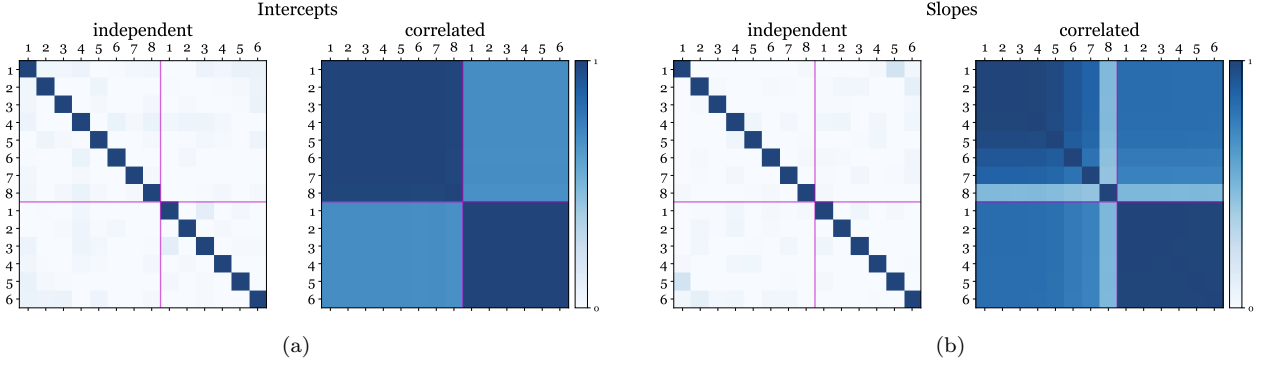


Figure 15: Pearson correlation coefficient of the conditional posterior distribution for the linear coefficients α_k (slopes and intercepts). Purple lines separate the alternator tasks (up to 8) and turbocharger tasks (up to 6).

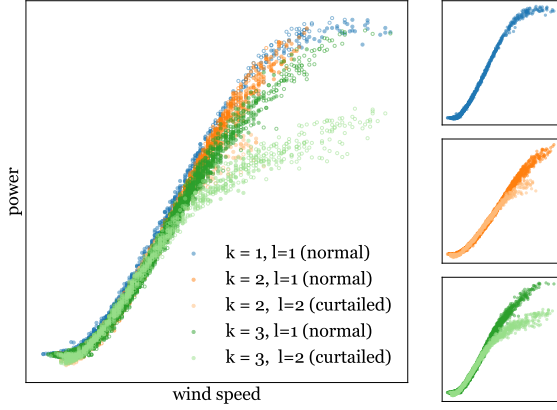


Figure 16: Power-curve data from three $k \in \{1, 2, 3\}$ wind turbines of the same make and model. Relationships correspond to normal $l = 1$ and ideal $l = 2$ operation.

where the fixed effects are **green** and the random effects are **purple**. Each segment of the regression could be presented in a similar formulation to (20), such that each component is a standard varying intercepts/slope model [15]. We avoid matrix notation, however, to present the model (and priors) around parameters $\{P_m, m_1, m_2, p, q, r\}$.

Given their interpretability, we can postulate weakly informative priors for each parameter. For the change points,

$$p \sim N(\mu_p, \sigma_{cp}^2), \quad q^{(kl)} \sim N(\mu_q, \sigma_{cp}^2), \quad r^{(kl)} \sim N(\mu_r, \sigma_{cp}^2)$$

$$\mu_p \sim N(.2, .5), \quad \mu_q \sim N(.4, .5), \quad \mu_r \sim N(.6, .5)$$

$$\sigma_{cp} \sim \text{IG}(1, 1) \quad (23)$$

These priors reflect that change points are expected to occur at regular intervals across the input domain with relatively high variance (relative to a normalised scale). The priors for gradient and maximum power are,

$$m_1^{(kl)} \sim N(\mu_{m_1}, \sigma_{m_1}^2)$$

$$\mu_{m_1} \sim N(2.5, .5), \quad \sigma_{m_1} \sim \text{IG}(1, 1) \quad (24)$$

$$P_m^{(1)} \sim N(1, .1), \quad P_m^{(2)} \sim N(.8, .1) \quad (25)$$

These distributions postulate the expected gradient m_2 in a normalised space; unit max power $P_m^{(1)}$ for normal operation; and a typical 80% curtailment [52] for the limited output $P_m^{(2)}$. No prior is required for m_2 since it is specified by $\{P_m, m_1, p, q, r\}$ in (22). As with the truck-fleet example, the $\text{IG}(1, 1)$ distributions weakly encourage inter-task correlations, such that the prior intentionally overestimates the deviation between task parameters.

6.3. Results

Figure 17 shows posterior predictive distribution from fleet-level inference – compared to independent models, plotted with light shading. Intuitively, variance reduction is most obvious for sparse or poorly described domains (orange and dark green). There is an overall increase in the predictive likelihood when fleet modelling, from 9620 to 9756. Table 3 quantifies changes in task-wise predictions – there is a likelihood increase in all domains other than $(k = 2, l = 1)$ and $(k = 3, l = 2)$. We believe reductions occur in these two domains as the model is constrained such that, to maximise the overall likelihood, the performance in data-rich domains is reduced in a trade-off. In other words, our prior belief is best suited to data-rich tasks – when the prior becomes more informed by data, it becomes less suitable in data-rich domains, and instead represents the population. (Consider that the overall likelihood increases, despite task-wise fluctuations.)

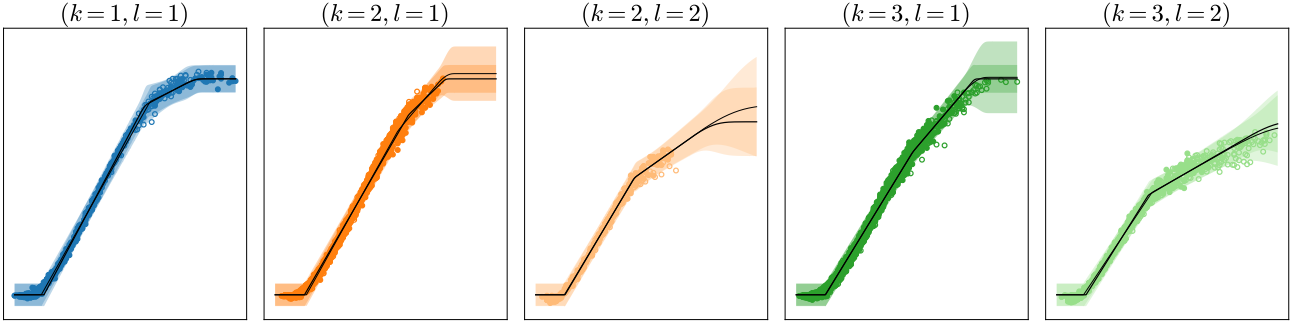


Figure 17: Posterior predictive distribution, the mean and three-sigma deviation for: (light shading, light line) K independent power-curve models $p(\mathbf{y}_{kl}^* | \mathbf{x}_{kl}^*, \mathbf{x}_{kl}, \mathbf{y}_{kl})$. (dark shading, thick line) multitask learning with mixed effects $p(\mathbf{y}_{kl}^* | \mathbf{x}_{kl}^*, \{\{\mathbf{x}_{kl}, \mathbf{y}_{kl}\}_{k=1}^{K_l}\}_{l=1}^L)$.

Table 3: Predictive log likelihood $\log p(\mathbf{y}_{kl}^* | \mathbf{x}_{kl}^*)$. Here l corresponds to the operating condition (normal $l = 1$, or curtailed $l = 2$) while k is turbine identifier.

model		$k = 1$	$k = 2$	$k = 3$
STL	normal ($l = 1$)	203	3151	5139
STL	curtailed ($l = 2$)	-	539	724
MTL	normal ($l = 1$)	217	2970	5201
MTL	curtailed ($l = 2$)	-	549	681

To combat this, uninformative priors should be considered [15]; these are discussed in Section 7.

Figure 18 shows the posterior distribution of the parameters inferred at the independent and fleet level. The cut-in speed q moves towards an average of the independent models, with reduced variance; this should be expected since q becomes tied as a population estimate. The change points q cluster intuitively, such that the normal and curtailed tasks form two groups (dark and light shades). The estimated r parameters are significantly improved through partial pooling – in particular, the green and orange domains shift much further from the weakly informative prior. There is a notable reduction in the variance across all tasks for the slope estimate m_2 .

Figure 19 presents insights relating to maximum power estimates P_m . The tied parameter for the normal maximum $P_m^{(k,1)}$ moves toward the data-rich estimate (blue), while the curtailed maximum $P_m^{(k,2)}$ moves toward an average of the relevant tasks (where $l = 2$). In both operating conditions, parameter tying enables the move from vague posteriors to distributions with clear expected values.

Finally, Figure 20 plots the Pearson correlation coefficient of the pair-wise conditionals of q between tasks. (q is presented since it is the most struc-

tured/insightful.) It is clear that, by moving to a hierarchical model, the correlation between similar tasks is appropriately captured, with two distinct blocks associated with the normal and curtailed groups.

7. Concluding Remarks

Hierarchical Bayesian modelling with mixed effects is demonstrated as an effective method of sharing information between models of fleets of assets in engineering. Parameter estimation and predictive capabilities are improved (for the combined fleet) in two case studies, utilising the same flexible multi-task learning framework. Important considerations are discussed when formulating each population model: prior elicitation, mixed-effects formulation, and negative transfer – these concepts are critical to the success of population-level inference.

The first case-study concerns the survival analysis of turbocharger and alternator components in an operational fleet of trucks (owned by Scania). A semi-parametric hazard curve model is improved through partial pooling and parameter tying – where selected parameters are inferred at the population-level, rather than vehicle subgroups. The method builds on engineering intuition since correlations in the hierarchy can be inspected to determine which groups of vehicles or components are similar (i.e. correlated) for which effects in the survival model (i.e. interpretable parameters).

The second study presents power prediction for a group of wind turbines. The SCADA monitoring data were provided by Visualwind, measured from the same model of turbine in different locations. Correlated power curve models are learnt as a segmented (piece-wise) linear regression, described by interpretable parameters. By moving to

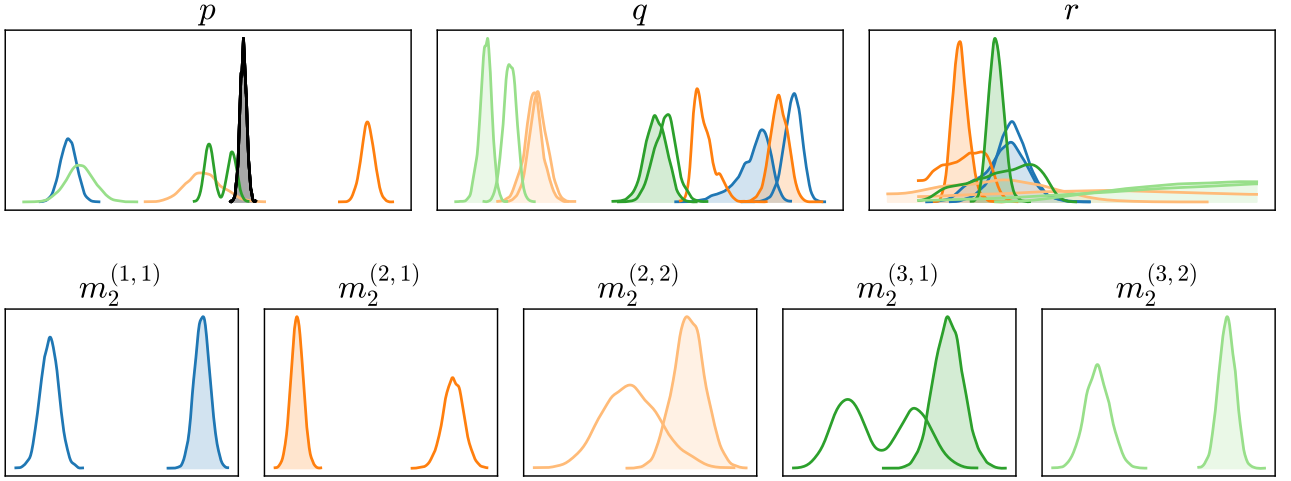


Figure 18: Changes in the posterior distribution: the cut-in speed p , initiation of curtailment q , rated speed r , and linear slope m_1 . Independent models (hollow) compared to population-level modelling (shaded). When the parameter is tied (or fixed) the distributions are black.

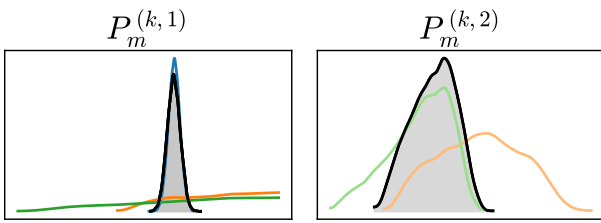


Figure 19: Changes in the posterior distribution of the: Independent models (hollow) compared to population-level modelling (shaded).

a population-level inference, parameter estimation is improved, as well as model generalisation (for the combined population estimates). In particular, the estimation of maximum power is significantly improved for turbines with fewer data and recently in operation.

The success of these models depends on the reliability of the domain knowledge encoded in the prior distributions. In this case, priors were postulated as weakly informative, since interpretable parameters and domain expertise allowed sensible prior elicitation. When such elicitation is infeasible, future work should consider the use of uninformative priors [54], especially for the (variance) parameters that control the level of correlation between related tasks.

Future work should also consider an objective method to categorise sub-fleet data in a practical setting; this might include clustering assets from specification or operations data. The labelling of data into distinct tasks can be non-trivial in an engineering setting and requires investigation.

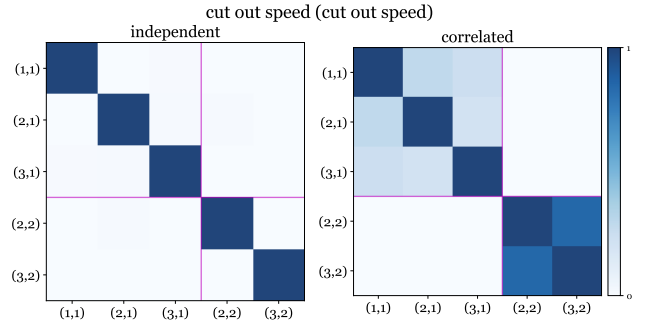


Figure 20: Pearson correlation coefficient of the conditional posterior distribution for the rated wind speed q , tick labels correspond to (k, l) . Purple lines separate the normal ($l = 1$) from the curtailed task-parameters ($l = 2$).

Acknowledgements

A.B. Duncan and L.A. Bull were supported by Wave 1 of The UKRI Strategic Priorities Fund under the EPSRC Grant EP/W006022/1, particularly the *Ecosystems of Digital Twins* theme within that grant and The Alan Turing Institute. M. Dhada was supported by the Next Generation Converged Digital Infrastructure project (EP/R004935/1) funded by the Engineering and Physical Sciences Research Council and BT. This research was supported by Scania CV (Sweden) and Visualwind (UK).

References

- [1] K. Worden and G. Manson. The application of machine learning to structural health monitoring. *Philosophical Transactions of the Royal Society A: Mathematical, Physical and Engineering Sciences*, 365(1851):515–537, 2007.

- [2] P. O'Connor and A. Kleyner. *Practical Reliability Engineering*. John Wiley & Sons, 2012.
- [3] N.-H. Kim, D. An, and J.-H. Choi. Prognostics and health management of engineering systems. *Switzerland: Springer International Publishing*, 2017.
- [4] A. Paleyes, R.-G. Urma, and N. D. Lawrence. Challenges in deploying machine learning: a survey of case studies. *arXiv preprint arXiv:2011.09926*, 2020.
- [5] L. Bull, T. Rogers, C. Wickramarachchi, E. Cross, K. Worden, and N. Dervilis. Probabilistic active learning: An online framework for structural health monitoring. *Mechanical Systems and Signal Processing*, 134:106294, 2019.
- [6] L. Bull, P. Gardner, J. Gosliga, T. Rogers, N. Dervilis, E. Cross, E. Papatheou, A. Maguire, C. Campos, and K. Worden. Foundations of population-based SHM, part I: Homogeneous populations and forms. *Mechanical Systems and Signal Processing*, 148:107141, 2021.
- [7] J. Gosliga, P. Gardner, L. Bull, N. Dervilis, and K. Worden. Foundations of population-based SHM, part II: Heterogeneous populations—graphs, networks, and communities. *Mechanical Systems and Signal Processing*, 148:107144, 2021.
- [8] P. Gardner, L. Bull, J. Gosliga, N. Dervilis, and K. Worden. Foundations of population-based SHM, part III: Heterogeneous populations—mapping and transfer. *Mechanical Systems and Signal Processing*, 149:107142, 2021.
- [9] V. Zaccaria, M. Stenfelt, I. Aslanidou, and K. G. Kyprianidis. Fleet monitoring and diagnostics framework based on digital twin of aero-engines. In *Turbo Expo: Power for Land, Sea, and Air*, volume 51128, page V006T05A021. American Society of Mechanical Engineers, 2018.
- [10] G. Michau and O. Fink. Domain adaptation for one-class classification: monitoring the health of critical systems under limited information. *arXiv preprint arXiv:1907.09204*, 2019.
- [11] L. Bull, P. Gardner, N. Dervilis, E. Papatheou, M. Haywood-Alexander, R. Mills, and K. Worden. On the transfer of damage detectors between structures: An experimental case study. *Journal of Sound and Vibration*, 501:116072, 2021.
- [12] P. Gardner, L. Bull, N. Dervilis, and K. Worden. Overcoming the problem of repair in structural health monitoring: Metric-informed transfer learning. *Journal of Sound and Vibration*, page 116245, 2021.
- [13] M. Dhada, M. Girolami, and A. K. Parlikad. Anomaly detection in a fleet of industrial assets with hierarchical statistical modeling. *Data-Centric Engineering*, 1, 2020.
- [14] M. Wand. Semiparametric regression and graphical models. *Australian & New Zealand Journal of Statistics*, 51(1):9–41, 2009.
- [15] A. Gelman, J. Carlin, H. Stern, D. Dunson, A. Vehtari, and D. Rubin. *Bayesian Data Analysis*. Chapman and Hall/CRC, third edition, 2013.
- [16] K. P. Murphy. *Machine Learning: A Probabilistic Perspective*. MIT press, 2012.
- [17] S. Dorafshan, R. J. Thomas, and M. Maguire. Comparison of deep convolutional neural networks and edge detectors for image-based crack detection in concrete. *Construction and Building Materials*, 186:1031–1045, 2018.
- [18] Y. Gao and K. M. Mosalam. Deep transfer learning for image-based structural damage recognition. *Computer-Aided Civil and Infrastructure Engineering*, 33(9):748–768, 2018.
- [19] K. Jang, N. Kim, and Y.-K. An. Deep learning-based autonomous concrete crack evaluation through hybrid image scanning. *Structural Health Monitoring*, 18(5-6):1722–1737, 2019.
- [20] W. Zhang, G. Peng, C. Li, Y. Chen, and Z. Zhang. A new deep learning model for fault diagnosis with good anti-noise and domain adaptation ability on raw vibration signals. *Sensors*, 17(2):425, 2017.
- [21] X. Li, W. Zhang, Q. Ding, and J.-Q. Sun. Multi-layer domain adaptation method for rolling bearing fault diagnosis. *Signal Processing*, 157: 180–197, 2019.
- [22] Q. Wang, G. Michau, and O. Fink. Domain adaptive transfer learning for fault diagnosis. In *2019 Prognostics and System Health Management Conference (PHM-Paris)*, pages 279–285. IEEE, 2019.

- [23] P. Gardner, X. Liu, and K. Worden. On the application of domain adaptation in structural health monitoring. *Mechanical Systems and Signal Processing*, 138:106550, 2020.
- [24] P. Gardner, R. Fuentes, N. Dervilis, C. Mineo, S. Pierce, E. Cross, and K. Worden. Machine learning at the interface of structural health monitoring and non-destructive evaluation. *Philosophical Transactions of the Royal Society A*, 378(2182):20190581, 2020.
- [25] P. Gardner, L. Bull, N. Dervilis, and K. Worden. On the application of kernelised bayesian transfer learning to population-based structural health monitoring. *Mechanical Systems and Signal Processing*, 167:108519, 2022.
- [26] Z. Sun, A. Barp, and F.-X. Briol. Vector-valued control variates. *arXiv preprint arXiv:2109.08944*, 2021.
- [27] H.-P. Wan and Y.-Q. Ni. Bayesian multi-task learning methodology for reconstruction of structural health monitoring data. *Structural Health Monitoring*, 18(4):1282–1309, 2019.
- [28] E. V. Bonilla, K. Chai, and C. Williams. Multi-task gaussian process prediction. *Advances in neural information processing systems*, 20, 2007.
- [29] Y. Li, T. Bao, Z. Chen, Z. Gao, X. Shu, and K. Zhang. A missing sensor measurement data reconstruction framework powered by multi-task gaussian process regression for dam structural health monitoring systems. *Measurement*, 186:110085, 2021.
- [30] P. Seshadri, A. Duncan, G. Thorne, G. Parks, R. V. Diaz, and M. Girolami. Bayesian assessments of aeroengine performance with transfer learning. *arXiv preprint arXiv:2011.14698*, 2020.
- [31] Y. Huang, J. L. Beck, and H. Li. Multitask sparse Bayesian learning with applications in structural health monitoring. *Computer-Aided Civil and Infrastructure Engineering*, 34(9):732–754, 2019.
- [32] Y. Huang and J. L. Beck. Hierarchical sparse Bayesian learning for structural health monitoring with incomplete modal data. *International Journal for Uncertainty Quantification*, 5(2), 2015.
- [33] D. Di Francesco, M. Chryssanthopoulos, M. H. Faber, and U. Bharadwaj. Decision-theoretic inspection planning using imperfect and incomplete data. *Data-Centric Engineering*, 2, 2021.
- [34] N. Papadimas and T. Dodwell. A hierarchical Bayesian approach for calibration of stochastic material models. *Data-Centric Engineering*, 2, 2021.
- [35] H. Daumé III. Bayesian multitask learning with latent hierarchies. *arXiv preprint arXiv:0907.0783*, 2009.
- [36] Y. Xue, X. Liao, L. Carin, and B. Krishnapuram. Multi-task learning for classification with dirichlet process priors. *Journal of Machine Learning Research*, 8(1), 2007.
- [37] I. G. Kreft and J. De Leeuw. *Introducing Multilevel Modeling*. Sage, 1998.
- [38] B. T. West, K. B. Welch, and A. T. Galecki. *Linear Mixed Models: A Practical Guide Using Statistical Software*. Chapman and Hall/CRC, 2006.
- [39] B. Carpenter, A. Gelman, M. D. Hoffman, D. Lee, B. Goodrich, M. Betancourt, M. Brubaker, J. Guo, P. Li, and A. Riddell. Stan: A probabilistic programming language. *Journal of statistical software*, 76(1), 2017.
- [40] M. D. Hoffman, A. Gelman, *et al.* The No-U-Turn sampler: adaptively setting path lengths in hamiltonian monte carlo. *J. Mach. Learn. Res.*, 15(1):1593–1623, 2014.
- [41] A. Birolini. *Reliability Engineering: Theory and Practice*. Springer Science & Business Media, 2013.
- [42] G. Rodriguez. Parametric survival models. *Princeton University, Rapport technique, Princeton*, 2010.
- [43] E. Papatheou, N. Dervilis, A. Maguire, C. Campos, I. Antoniadou, and K. Worden. Performance monitoring of a wind turbine using extreme function theory. *Renewable Energy*, 113:1490–1502, 2017.
- [44] T. Rogers, P. Gardner, N. Dervilis, K. Worden, A. Maguire, E. Papatheou, and E. Cross. Probabilistic modelling of wind turbine power curves with application of heteroscedastic Gaussian process regression. *Renewable Energy*, 148:1124 – 1136, 2020.
- [45] W. Yang, R. Court, and J. Jiang. Wind tur-

bine condition monitoring by the approach of SCADA data analysis. *Renewable Energy*, 53: 365–376, 2013.

- [46] V. Thapar, G. Agnihotri, and V. K. Sethi. Critical analysis of methods for mathematical modelling of wind turbines. *Renewable Energy*, 36 (11):3166–3177, 2011.
- [47] C. Carrillo, A. O. Montaña, J. Cidrás, and E. Díaz-Dorado. Review of power curve modelling for wind turbines. *Renewable and Sustainable Energy Reviews*, 21:572–581, 2013.
- [48] M. Lydia, S. S. Kumar, A. I. Selvakumar, and G. E. P. Kumar. A comprehensive review on wind turbine power curve modeling techniques. *Renewable and Sustainable Energy Reviews*, 30: 452–460, 2014.
- [49] M. Waite and V. Modi. Modeling wind power curtailment with increased capacity in a regional electricity grid supplying a dense urban demand. *Applied Energy*, 183:299–317, 2016.
- [50] S.-h. Hur and W. Leithead. Curtailment of wind farm power output through flexible turbine operation using wind farm control. *European Wind Energy Association Annual Event (EWEA 2014)*, pages 1–9, 2014.
- [51] M. Bontekoning, S. S. Perez-Moreno, B. Ummels, and M. Zaaier. Analysis of the reduced wake effect for available wind power calculation during curtailment. In *Journal of Physics: Conference Series*, volume 854, page 012004. IOP Publishing, 2017.
- [52] L. Bull, P. Gardner, T. Rogers, N. Dervilis, E. Cross, E. Papatheou, A. Maguire, C. Campos, and K. Worden. Bayesian modelling of multivalued power curves from an operational wind farm. *Mechanical Systems and Signal Processing*, page 108530, 2021.
- [53] M. M. Breunig, H.-P. Kriegel, R. T. Ng, and J. Sander. Lof: identifying density-based local outliers. In *Proceedings of the 2000 ACM SIGMOD international conference on Management of data*, pages 93–104, 2000.
- [54] A. Gelman. Prior distributions for variance parameters in hierarchical models. *Bayesian analysis*, 1(3):515–534, 2006.

Appendix A. B-splines

Assuming uniform knot locations $x_{h+k} = x_h + \delta k$, cubic B-splines are defined as the following piecewise cubic polynomial [15],

$$b_h(x) = \begin{cases} \frac{1}{6}u^3 & x \in (x_h, x_{h+1}), \quad u = (x - x_h)/\delta \\ \frac{1}{6}(1 + 3u + 3u^2 - 3u^3) & x \in (x_{h+1}, x_{h+2}), \quad u = (x - x_{h+1})/\delta \\ \frac{1}{6}(4 - 6u^2 + 3u^3) & x \in (x_{h+2}, x_{h+3}), \quad u = (x - x_{h+2})/\delta \\ \frac{1}{6}(1 - 3u + 3u^2 - u^3) & x \in (x_{h+3}, x_{h+4}), \quad u = (x - x_{h+3})/\delta \\ 0 & \text{otherwise} \end{cases} \quad (\text{A.1})$$

Appendix B. Cross validation Scania

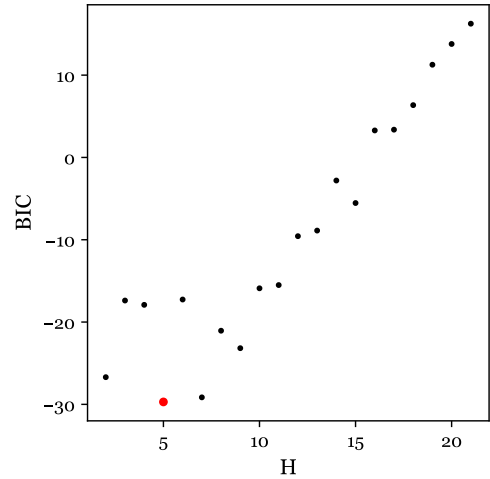


Figure B.21: Validation of an appropriate number of splines using the Bayesian Information Criterion (BIC) and 20-fold cross-validation. The best model $H = 5$ is highlighted with a red marker.

Appendix C. Segmented (piece-wise) power curve model

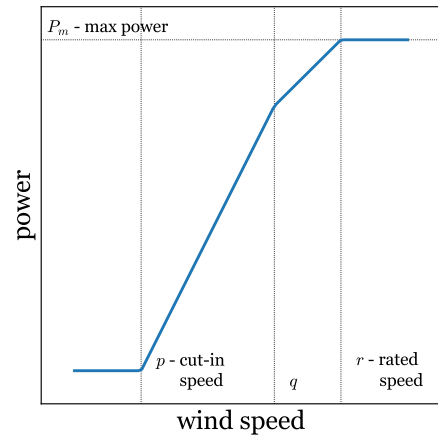


Figure C.22: The segmented linear power-curve model, indicating interpretable parameters $\{p, q, r, P_m\}$.

Appendix D. Turbocharger model: consistent model formulation

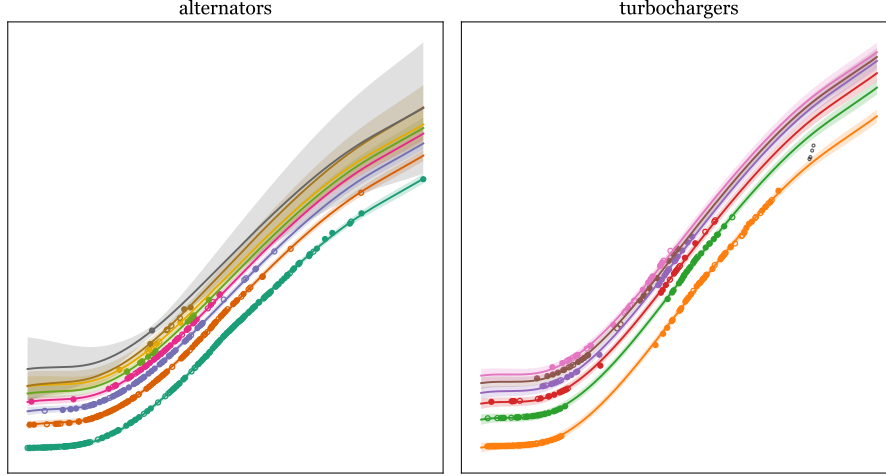


Figure D.23: Posterior predictive distribution $p(\mathbf{y}_k^* | \mathbf{x}_k^*, \{\mathbf{x}_k, \mathbf{y}_k\}_{k=1}^K)$: the mean and three-sigma deviation for multitask learning with mixed effects.

Appendix E. Turbocharger model: variance reduction plots

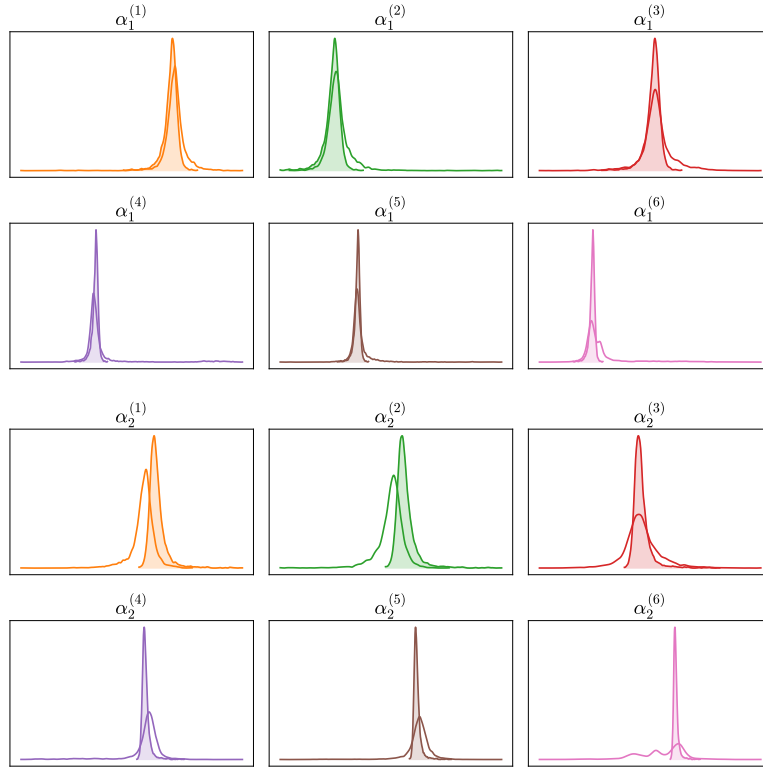


Figure E.24: Variance reduction in the posterior distribution of the intercept $\alpha_1^{(k)}$ and slope $\alpha_2^{(k)}$ parameters. Independent models (hollow) / population-level modelling (shaded).